Environmental Science and Pollution Research
https://doi.org/10.1007/s11356-021-14636-5

RESEARCH ARTICLE

Cytotoxicity, oxidative stress, and apoptosis in human embryonic kidney (HEK293) and colon cancer (SW480) cell lines exposed to nanoscale zeolitic imidazolate framework 8 (ZIF-8)

Seyed Ali Johari[1,2] · Mehrdad Sarkheil[3] · Shakila Veisi[1]

Received: 8 April 2021 / Accepted: 26 May 2021

Abstract

Zinc (zeolitic) imidazolate framework 8 (ZIF-8) has been widely considered in the literature as an ideal candidate for drug delivery especially anti-cancer drugs. However, the available information on the biocompatibility and cytotoxicity of ZIF-8 nanoparticles is contradictory. Therefore, in the present study, the ZIF-8 particles were synthetized, characterized, and their potential toxicity on two eukaryotic cell lines including human embryonic kidney (HEK293) and human colon cancer (SW480) cells was investigated in vitro. The characterization of ZIF-8 particles by TEM, EDX, SEM, and DLS indicated the synthesis of the hexagonal crystals with mean diameter of 124.71±32.74 nm and the presence of the zinc element at 86.25% by weight (wt%) of the ZIF-8 structure. The results of the cytotoxicity assessment of ZIF-8 NPs showed that the viability of two different cell lines reduced significantly coincident with increasing exposure concentration from 0 to 500 μg mL^{-1} ($P<0.05$). The 24-h half-inhibitory concentration (IC50-24 h) values of ZIF-8 NPs for HEK293 and SW480 cell lines were 116.22 and 36.23 μg mL^{-1}, respectively. We found that the viability of SW480 cells was significantly lower than the HEK293 cells in all exposure concentrations of ZIF-8 NPs except control. Exposure of both cells resulted in increasing of the intracellular reactive oxygen species (ROS) production and activation of apoptosis pathway. The apoptosis rate of cancer SW480 cells was higher than the normal HEK293 cells. These findings indicate that synthetized ZIF-8 NPs could be a candidate for cancer therapy, although their toxic effects on the normal cells also should be considered.

Keywords Anti-cancer · Antineoplastic · Apoptosis · Cytotoxicity · Reactive oxygen species · Zeolitic imidazolate framework

Introduction

Cancer has been known as one of leading causes of death in the recent decades (Nel et al. 2009; Liu et al. 2018). Chemotherapy is a common therapeutic approach for combating cancer, but the efficiency of various anti-cancer therapeutic agents is curbed by several limitations including low solubility, reduced bioavailability, high toxicity toward the normal cells, rapid clearance and drug resistance (Jaracz et al. 2005; Heath and Davis 2008; Wicki et al. 2015; Zarogoulidis et al. 2012). Hence, there is a necessary need to design and develop new anti-cancer agents to reduce many of undesirable problems and outcomes of conventional chemotherapy.

Nanoparticle-based drugs because of enhanced permeability and retention (EPR) effect have recently developed to improve drug accumulations at the tumor location (Kumar et al. 2018; Li et al. 2018; Wang et al. 2017). It is well known that the entry of nanoparticles to live cells often occurs either through endocytosis mechanisms or passive penetration of plasma membrane as alternative pathway (Wang et al. 2012; Salatin and Yari Khosroushahi 2017). Nanoscale metal-organic frameworks (MOFs) have recently received much attention as a novel therapeutic agent in biomedical fields (Chen et al. 2018; Liu et al. 2018). MOFs are defined as porous hybrid materials with specific properties such as large surface area, extreme pore volume, variety of sizes and shapes and tunable functional groups within

Responsible Editor: Lotfi Aleya

✉ Seyed Ali Johari
a.johari@uok.ac.ir; sajohari@gmail.com

[1] Department of Fisheries, Faculty of Natural Resources, University of Kurdistan, P.O. Box 416, Sanandaj 66177-15175, Iran

[2] Department of Zrebar Lake Environmental Research, Kurdistan Studies Institute, University of Kurdistan, Sanandaj, Iran

[3] Department of Fisheries, Faculty of Natural Resources and Environment, Ferdowsi University of Mashhad, Mashhad, Iran

Published online: 01 June 2021

the organic linker of frameworks (Liu et al. 2018; Peng et al. 2018). In addition to the application of MOFs in drug delivery, they are also used in various environmental sectors such as absorbing and adsorbing pollutants, environmental contaminant sensing, catalysis, gas storage, gas separation, and so on (Fang et al. 2018; Khan et al. 2020).

Zeolitic imidazolate framework-8 (ZIF-8) is known as a subclass of MOFs and is built from zinc ions and four 2-methyl imidazolate groups, which are components of physiological systems (Nabipour et al. 2017; Liu et al. 2018). ZIF-8 is a pH-responsive material that can be decomposed at an acidic pH environment like cancer cells which are more acidic (pH 5.7–7.8) than normal cells (Sun et al. 2012; Zhuang et al. 2014; Chen et al. 2018); thus, it can be considered an ideal candidate for cancer therapy. It has been shown that toxicity of DOX@ZIF-8 on breast cancer cells was higher than that of free DOX (Zheng et al. 2016). Due to the importance role of zinc in cancer prevention (Song and Ho 2009; Costello and Franklin 2013; Pavithra et al. 2015), slow and controlled release of zinc from ZIF-8 nanocrystals can effectively improve its anti-cancer properties (Ran et al. 2018). Hoop et al. (2018) found that cytotoxicity of ZIF-8 nanoparticles on six different cell lines at concentrations of above 30 μg mL^{-1} was due to the effect of released zinc ions on the mitochondrial reactive oxygen species (ROS) generation, DNA damage and eventually activation of apoptosis pathways. Apart from being used in anti-cancer drug delivery, many studies have shown that ZIF-8 has a very high ability to remove organic and mineral pollutants as well as antibiotics from municipal water and wastewater (Li et al. 2019; Liu et al. 2019; Zhou et al. 2019; Huang et al. 2020; Jampa et al. 2020). In addition, Taheri et al. (2021) showed that ZIF-8 has a very high antibacterial potential against gram-negative bacteria, *E. coli*.

Despite the many advantages of ZIF-8 and other MOF materials for drug delivery applications, the existing literature regarding their biocompatibility and cytotoxicity assessments are contradictory (Vasconcelos et al. 2012; Tamames-Tabar et al. 2014; Grall et al. 2015; Sajid 2016). It is necessary to determine the biocompatibility and toxicity potential of synthetized MOFs toward different normal and cancer cell lines in vitro conditions before their use in vivo. Therefore, in this study, we aimed to synthetize ZIF-8 nanoparticles and evaluate their potential toxicity on two eukaryotic cell lines including human embryonic kidney (HEK293) and human colon cancer (SW480) cells in vitro through determining cell viability, ROS production, and necrosis/apoptosis cells.

Materials and methods

Materials

Chemical materials including zinc nitrate hexahydrate ($Zn(NO_3)_2{\cdot}6H_2O$), 2-methylimidazole ($C_4H_6N_2$), and methanol were purchased from Merck. Acridine Orange/Propidium Iodide (AO/PI) solution was purchased from Sigma-Aldrich (St. Louis, MO, USA).

Synthesis of ZIF-8

The nanoscale ZIF-8 particles were synthesized based on the modified method described by Zheng et al. (2015). To prepare ZIF-8 particles, a solution of 2.4 g of zinc nitrate hexahydrate ($Zn(NO_3)_2{\cdot}6H_2O$) in 80 mL of deionized water was added drop-wise to a solution of 5.28 g of 2-methylimidazole ($C_4H_6N_2$) in 160 mL of methanol under stirring condition. The appearance of white color in the reaction solution represented the formation of ZIF-8 particles. The ZIF-8 particles were obtained by sonicating the solution for 20 min using probe sonicator (FAPAN 150UT, FAPAN CO. Ltd.) and then centrifuging for 15 min at 8000 rpm and 15 °C (Eppendorf 5804R, Germany). Afterwards, the white precipitate obtained was washed with methanol (90 mL for each time), sonicated and centrifuged three times. The synthetized particles were then dried in a freeze dryer (Dena Vacuum, FD-5005-BT, Iran) for further usage.

Characterization of synthetized ZIF-8

Transmission electron microscopy (TEM) was performed using transmission electron microscope (FE-TEM, JEM2100F, JEOL, Tokyo, Japan) equipped with an EDX (EDX, TM200, Oxford Instruments plc, Oxfordshire, UK) at an acceleration voltage of 200 k V. The ZIF-8 samples for TEM were prepared by dissolving 10 mg of particles in 5 mL of ethanol alcohol (EtOH), sonicating for 5 minutes and drying on a drop per TEM grid (Quantifoil 656-200-Cu, Tedpella, Inc., Redding, CA). Scanning electron microscope (SEM) images were obtained using a MIRA3 SEM (Tescan, Czech Republic). Dynamic light scattering (DLS) analysis was performed using VASCO^{TM} nanoparticle size analyzer (Cordouan Technologies, France). Zeta potential of synthetized particles was measured using SZ-100 (HORIBA, Japan) with holder temperature of 24.9 °C.

Cell culture

Human embryonic kidney (HEK293) and human colon cancer (SW480) cell lines were purchased from the American Type Culture Collection (ATCC, Manassas, VA, USA) and were grown in DMEM cell culture medium supplemented with 10% fetal bovine serum (FBS) and 1% penicillin-streptomycin.

MTT–cell viability assay

MTT assay was performed based on the method explained by Bigdeli et al. (2019). The HEK293 and SW480 cells were

separately seeded on 96-well plates (SPL Life Sciences, South Korea) at a density of 1×10^4 cells per well that filled with the cell medium DMEM supplemented with 10% FCS and 1% antibiotics. The cells were grown for 24 h and then, exposed to the different concentrations (0, 15.625, 31.25, 62.5, 125, 250, and 500 μg mL^{-1}) of ZIF-8 for 24 h. Afterwards, 0.05 mL of MTT solution was added to each well and incubated at 37 °C for 4 h and during this time a purple colored formazan crystal was formed. The crystals were dissolved by adding 100 μL of DMSO and the absorbance of solution was measured at a wavelength of 570 nm using a plate reader (Bio-Rad, Hercules, CA).

Live/dead cell staining

Each of HEK293 and SW480 cells were separately seeded at a density of 10^6 cells mL^{-1} in 25 cm^2 culture flask and incubated for 24 h. In following, the cells were exposed with 1.5-fold of IC50 concentration of ZIF-8 NPs determined by MTT assay (174.33 and 54.34 μg mL^{-1} for HEK293 and SW480, respectively) for 24 h. After exposure period, the supernatant was collected and transferred into a falcon tube. The remaining cells in the flask were also trypsinized and collected using a scraper. The collected cells were resuspended using 2 mL of PBS and then, added to falcon tube containing the supernatant. In next step, the cells were centrifuged at 300 g for 5 min and the obtained supernatant was discharged and the cells were rinsed with 5 mL of PBS. This step repeated again and the falcon tube kept in ice. AO/PI (Sigma-Aldrich) (1 mL) as a dye mixture was diluted with PBS (1 mL) under dark conditions. The prepared AO/PI solution was added to 10 μL aliquot of cells and the mixture was transferred on to a slide. Fluorescence images were taken by a UV-fluorescent microscope equipped with 20 objective lenses (Axio Scope A1, Zeiss, Oberkochen, Germany).

Reactive oxygen species (ROS) assay

The amount of intracellular ROS production was determined based on flow cytometry technique using ROS detection assay kit (Abcam Inc., USA). The HEK293 and SW480 cells were separately seeded into a 6-well plate at a density of 1×10^6 cells/mL and treated with 1.5-fold of IC_{50} of ZIF-8 NPs determined by MTT assay (174.33 and 54.34 μg/mL for HEK293 and SW480, respectively) for 24 h. Untreated cells were considered control. After treatment, 2′,7′-dichlorofluorescein diacetate (DCF-DA) dye (20 μM) was added to each well and then, the cells were incubated at 37 °C for 30 min under dark conditions. The ROS production was quantified with excitation and emission wavelengths at 485 and 535 nm respectively.

Annexin V-FITC/PI assay

The population of necrosis and apoptotic cells was quantified using Annexin V-FITC/PI staining kit. Firstly, the cells were seeded in 6-well plates at a density of 1×10^6 cells/mL and then, exposed to ZIF-8 NPs at concentration of 1.5 fold of IC50 (174.33 and 54.34 μg/mL for HEK293 and SW480, respectively) for 24 h. Afterwards, the treated cells were dispersed using the binding buffer and incubated with 20 μL of Annexin V-FITC and PI for 15 min in dark conditions. After staining, the amounts of viable, early apoptotic, late apoptotic, and necrotic cells were measured using flow cytometry.

Statistical analysis

The data were presented as mean ± SD. The statistical analysis of data was carried out using SPSS software (Version, 19). Normality assumption of data was investigated using Kolmogorov-Smirnov test. Significant differences between the means were evaluated using one-way analysis of variance (ANOVA) followed by the Duncan multiple range test. The independent-sample *T* test was used to determine the significant difference between the two independent samples. The *P*-value of <0.05 was employed to assay the significant differences.

Results and discussion

Characterization of ZIF-8

The morphology, size, and elemental composition of synthetized ZIF-8 nanoparticles (NPs) were determined by TEM and EDX (Fig. 1a, b). TEM and SEM images indicate the formation of hexagonal crystals (Figs. 1a and 2a). The EDX analysis confirmed the presence of the zinc and oxygen elements at 86.25% and 13.75% by weight (wt%) of the ZIF-8 structure, respectively. Hoop et al. (2018) also confirmed that Zn element uniformly distributed throughout of ZIF-8 crystals with average diameter of 1.1 μm.

Measurement of the diameter of 312 particles in SEM micrograph of ZIF-8 NPS revealed the uniform sizes of particles with mean diameter of 124.71±32.74 nm and size distribution ranged from 38.36 to 236.21 nm (Fig. 2b). The average size of synthetized crystals was approximately consistent with those previously reported (Zheng et al. 2015; Tiwari et al. 2017; Ran et al. 2018; Jin et al. 2020). Nano-size drugs are efficiently taken up and accumulated in cancer cells through endocytosis and subsequently kill the cells, while macromolecular drugs are entered the cancer cells just via molecular diffusion (Liu et al. 2018). The size of nanoparticles efficiently affects cellular endocytosis mechanism (Li et al. 2015), as smaller

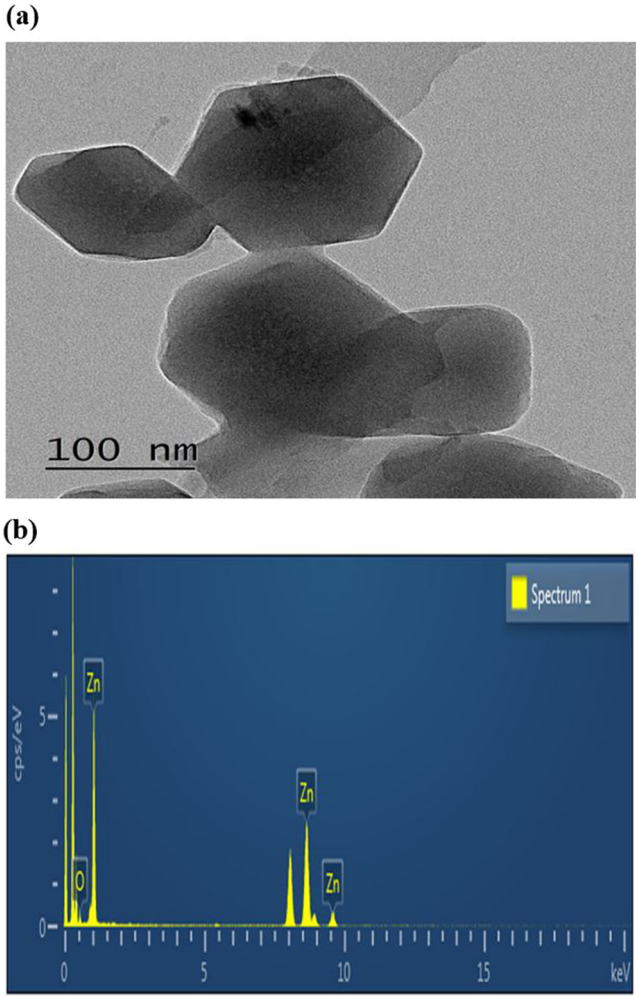

Fig. 1 TEM micrograph (a) and EDX spectrum (b) of ZIF-8 nanoparticles

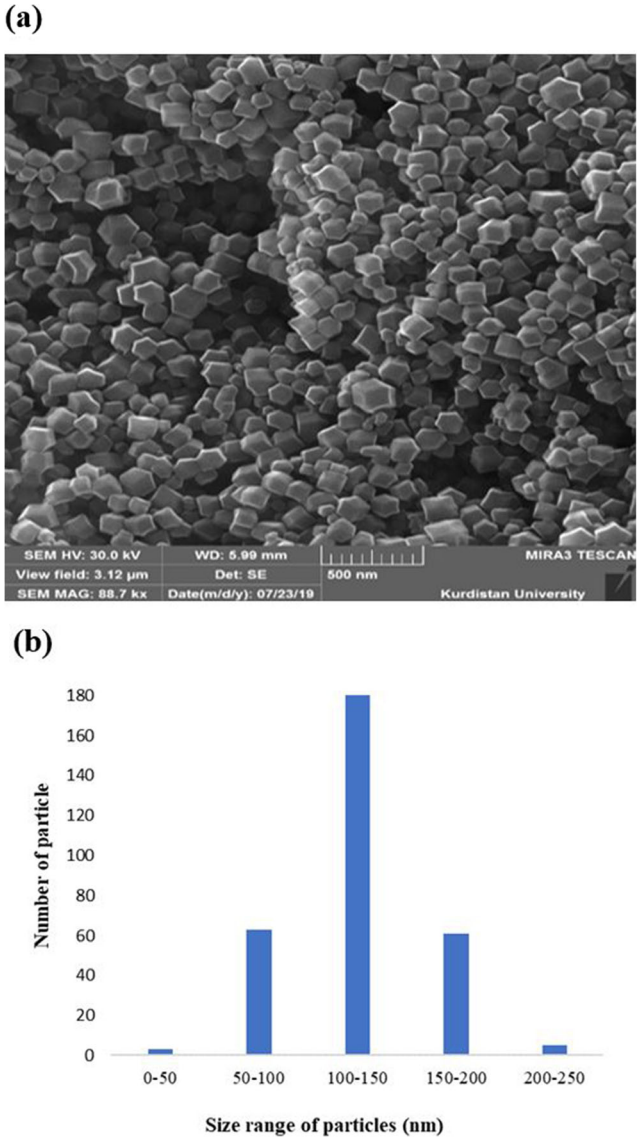

Fig. 2 SEM micrograph (a) and size distribution of ZIF-8 nanoparticles (b)

particles are more easily taken up by cells (Chuah et al. 2014). In addition, nanoparticles have a larger surface area than larger particle, which allows them to have more contact with cell membranes (De Jong and Borm 2008).

The hydrodynamic particle sizes of synthetized ZIF-8 NPs were further studied by dynamic light scattering (DLS) analysis (Fig. 3a, b). According to Padé-Laplace algorithm, number intensity of particles with 74.39 and 236.32 nm in the ZIF-8 suspension was 98% and 2 %, respectively (Fig. 3a). Sparse Bayesian Learning (SBL) algorithms on DLS data revealed that the mean intensity of particles was 221.14 nm and the intensity of particles with 253.35 and 100.59 nm in the ZIF-8 suspension was 75.31% and 24.69 %, respectively (Fig. 3b). Zeta potential of prepared nanoparticles was measured to determine the surface charge of particles. The ZIF-8 NPs showed a negatively charged surface with a zeta potential of −25.2 mV. Nanomaterials with more negative potential under different physiological conditions display good colloidal stability (Liu et al. 2016; Shu et al. 2018).

Cytotoxicity assessment of ZIF-8 NPs

In order to determine the cytotoxicity of synthetized ZIF-8 NPs to eukaryotic cell lines, we assessed the effects of different concentrations of ZIF-8 NPs (0–500 μg mL^{-1}) on viability of the human embryonic kidney (HEK293) and human colon cancer (SW480) cell lines using MTT assay (Fig. 4). Cytotoxicity of ZIF-8 NPs was dependent on the cell type and on the concentration. The toxicity of ZIF-8 NPs on each cell line increased coincident with increasing exposure concentration from 0 μg mL^{-1} to 500 μg mL^{-1}. Hoop et al. (2018) examined the various concentrations of ZIF-8 NPs on six different human cell lines. They found that the viability of cells exposed to ZIF-8 concentrations of up to 30 μg mL^{-1} were approximately 80%, but the cell viability decreased to 10% for both 75 and 100 μg mL^{-1}. Zheng et al. (2015) also reported

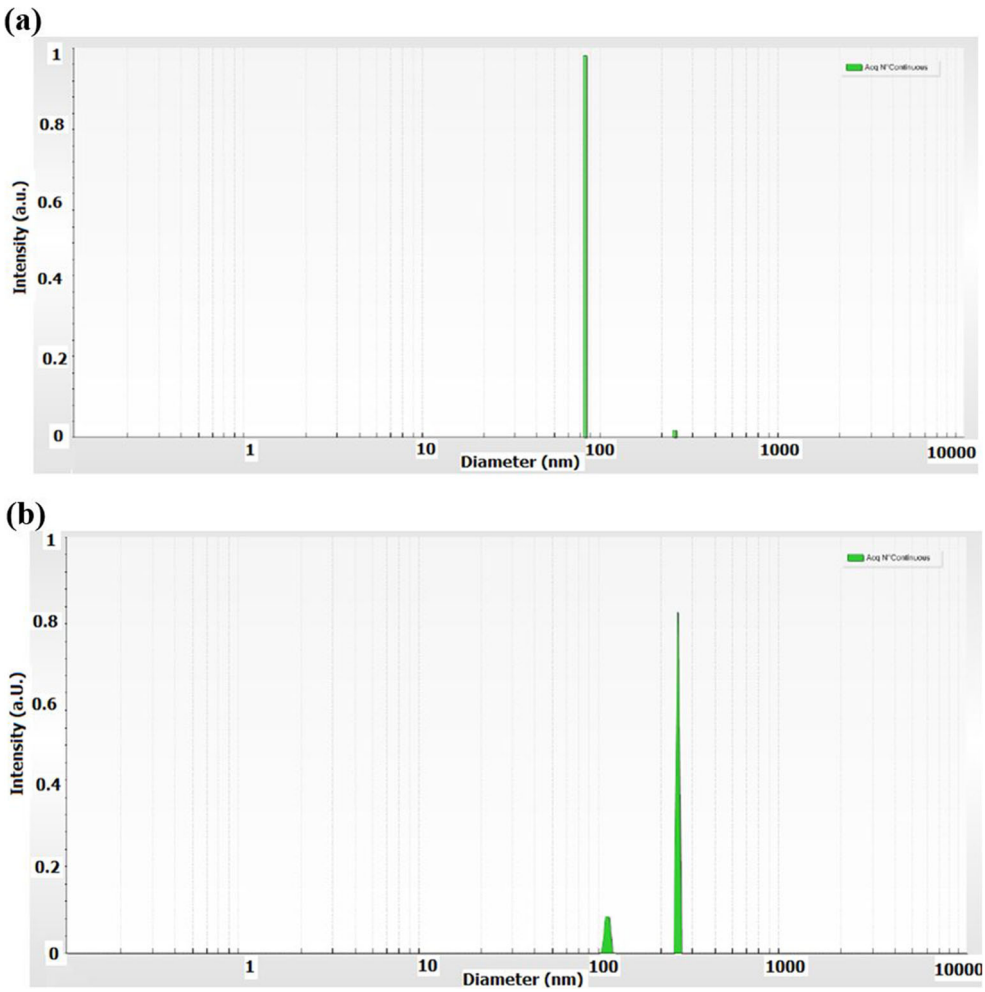

Fig. 3 Size distribution of ZIF-8 nanoparticles based on cumulant analysis (a) and sparse Bayesian Learning (SBL) algorithms (b) of dynamic light scattering (DLS) technique

that the survival rate of HeLa cells incubated with nanoscale ZIF-8 concentrations from 10 to 50 μg mL^{-1} for 48 h was above 70% compared to the control group. It was also shown that ZIF-8 (140 nm) had no obvious cytotoxicity effect on HeLa cells at concentrations below 50 μg mL^{-1} (Tiwari et al. 2017). In the present study, the exposure of HEK293 cells to ZIF-8-NPs had no significant effect on cell viability up to concentration of 62.5 μg mL^{-1}, but increasing exposure concentration to 125 μg mL^{-1} led to a significant cell viability reduction to 36.69% compared to the control (100%). For

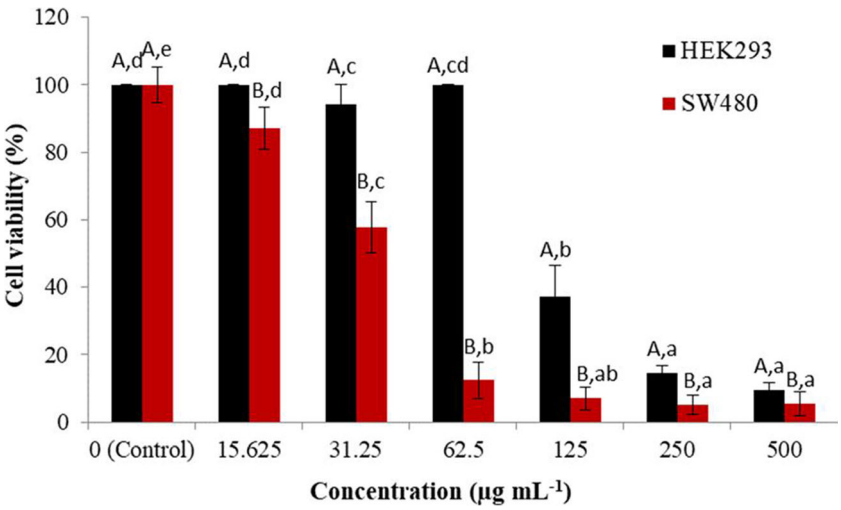

Fig. 4 Comparison of MTT cell viability of human embryonic kidney (HEK293) and human colon cancer (SW480) cells after exposure to different concentrations of ZIF-8 NPs for 24 h. Bars with different capital letters in each concentration are significantly different (mean ± SD, independent-sample *T* test, $P<0.05$). Bars with different lowercase letters in each cell line are significantly different (mean ± SD, one-way ANOVA, $P<0.05$)

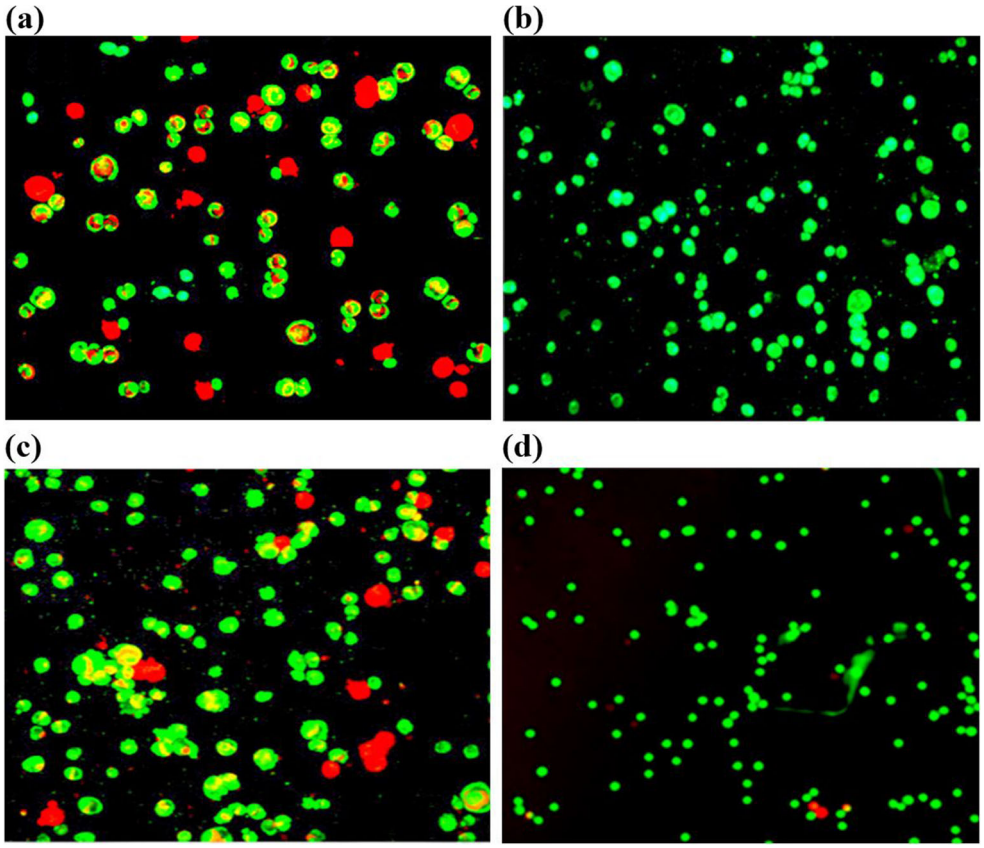

Fig. 5 Live/dead assay of human colon cancer (SW480) and human embryonic kidney (HEK293) after incubation with ZIF-8 NPs for 24 h. SW480 cells were exposed to 1.5-fold of IC50 concentration of ZIF-8 NPs (54.34 μg mL^{-1}) (a) compared to 0 mg/L of ZIF-8 NPs (control) (b) and HEK293 cells treated with 1.5-fold of IC50 concentration of ZIF-8 NPs (174.33 μg mL^{-1}) (c) compared to a control group (d). Viable cells (green fluorescence) and dead cells (red fluorescence) were determined by AO/PI staining

SW480 cells, the elevation of exposure concentration from 0 to 125 μg mL^{-1} of ZIF-8 NPs decreased the cell viability from 100 to 7.06%. The highest inhibitory effect of ZIF-8 NPs on both cell lines was observed at 250 and 500 μg mL^{-1}. Based on the cytotoxic activity of ZIF-8 nanocrystals using cancer MCF-7 cell line, total inhibition of cell viability was achieved at concentration of 250 μg mL^{-1} (Ran et al. 2018). The influence of ZIF-8 concentrations on cell viability may be attributed to release of Zn^{2+} into the cell media, which induce ROS generation and ultimately a cell cycle arrest in G2/M and activation of apoptosis pathways (Cadet and Wagner 2013; Clausen et al. 2013; Hoop et al. 2018). However, since the current study did not evaluate the release of Zn ions into the cell media, the findings should be judged with caution and further study need to be done to examine the toxicity mechanisms of ZIF-8 NPs.

The susceptibility of each cell line to ZIF-8 NPs was determined by calculating the 24-h half-inhibitory concentration (IC50-24 h). Based on the results of the cell viability and proliferation response, the IC50-24 h values of ZIF-8 NPs for HEK293 and SW480 cell lines were 116.22 and 36.23 μg mL^{-1}, respectively. The half-maximal effective concentration (EC50) of nanoscale ZIF-8 (110 nm) for HeLa cells was determined to be 63.8 μg mL^{-1} (Zheng et al. 2015). Vasconcelos et al. (2012) also reported that IC50 values of ZIF-8 (200 nm) for NCI, HT-29 and HL-60 cell lines were above 25 μg mL^{-1}. The results of present study demonstrated more sensitivity of SW480 cancer cells to ZIF-NPs than HEK293 normal cells. The comparison of viability of two cell lines in each exposure concentration showed that the viability of SW480 cell was significantly lower than the HEK293 cell except for 0 μg mL^{-1} of ZIF-8 NPs (Fig. 4). Most nano-sized agents preferentially accumulate and retain in cancer tissues compared with normal tissues due to the enhanced permeability and retention (EPR) effect, which induce greater therapeutic effects (Maeda 2001; Kobayashi et al. 2014). Some initial evidences have indicated that zinc has important role in cancer prevention (Hoang et al. 2016; Ran et al. 2018); however, there is little information on efficiency of zinc-derived compounds for cancer therapy. Ran et al. (2018) investigated the cytotoxicity of ZIF-8 nanocrystals with normal model cell line HEK293 and colon cancer cell line HCT8. They found a very low toxicity of ZIF-8 for the normal cells, but the inhibitory effect of ZIF-8 on cancer HCT8 cells. This phenomenon was attributed to the zinc released from ZIF-8 (25.41 μmol L^{-1}) and more absorption of zinc due to the increased permeability of the cancer cells.

To confirm the viable and dead cells of human colon cancer (SW480) and human embryonic kidney (HEK293) incubated with ZIF-8 NPs for 24 h, a live/dead staining assay was

conducted. Acridine Orange (AO) and Propidium Iodide (PI) dyes were used to discriminate between live and dead cells. In cells stained with both dyes, live nucleated cells fluoresce green and dead nucleated cells fluoresce red. Untreated SW480 and HEK293 cells showed round-shape with green fluorescence, indicating the presence of viable cells (Fig. 5 b and d). After 24-h treatment with ZIF-8 NPs, the red fluorescence was clearly observed and greater red fluorescence was detected in the colon cancer SW480 cells than in the normal HEK293 cells (Fig. 5 a and c). Increased number of dead cells is probably in response to the ZIF-8 NP-induced formation of intracellular ROS and subsequently activation of apoptosis pathway.

Figure 6 represents the intracellular production of ROS in human colon cancer (SW480) and human embryonic kidney (HEK293) cell lines exposed to 1.5-fold of IC50 concentrations of ZIF-8 NPs and incubated with DCFH dye. The DCFH-DA fluorescence intensity in untreated SW480 cells was 2.25% and this value increased to 69.2% in treated cells, indicating the effect of ZIF-8 NPs on ROS production. Exposure of the HEK293 cells to 174.33 μg mL^{-1} (1.5-fold IC50) of ZIF-8 NPs resulted in increasing of the DCFH-DA fluorescence intensity to 79.5%, while this value was 4.08% in un-exposed cells. These results show that the ZIF-8 NPs obviously increase the intracellular ROS level in both cell lines. Hoop et al. (2018) found that increased ZIF-8 crystal in the cell culture of six different cell lines was associate with increasing Zn^{2+}, leading to an increment of intracellular ROS. Other researchers have also reported the dependency of ROS generation and intracellular Zn^{2+} concentrations (Link and von Jagow 1995; Dineley et al. 2003; Clausen et al. 2013). The ROS generation plays an important role in proliferation and survival of cell (Ding et al. 2016; Wasim and Chopra 2018). Shyamsivappan et al. (2020) reported that increased the production of ROS suppressed the growth of Breast cancer MCF7 cells through inducing G1/S and G2/M phase cell cycle arrest and promoting apoptosis. Utilization of GOx@Pd@ZIF-8 as a ROS generator to treat lung cancer

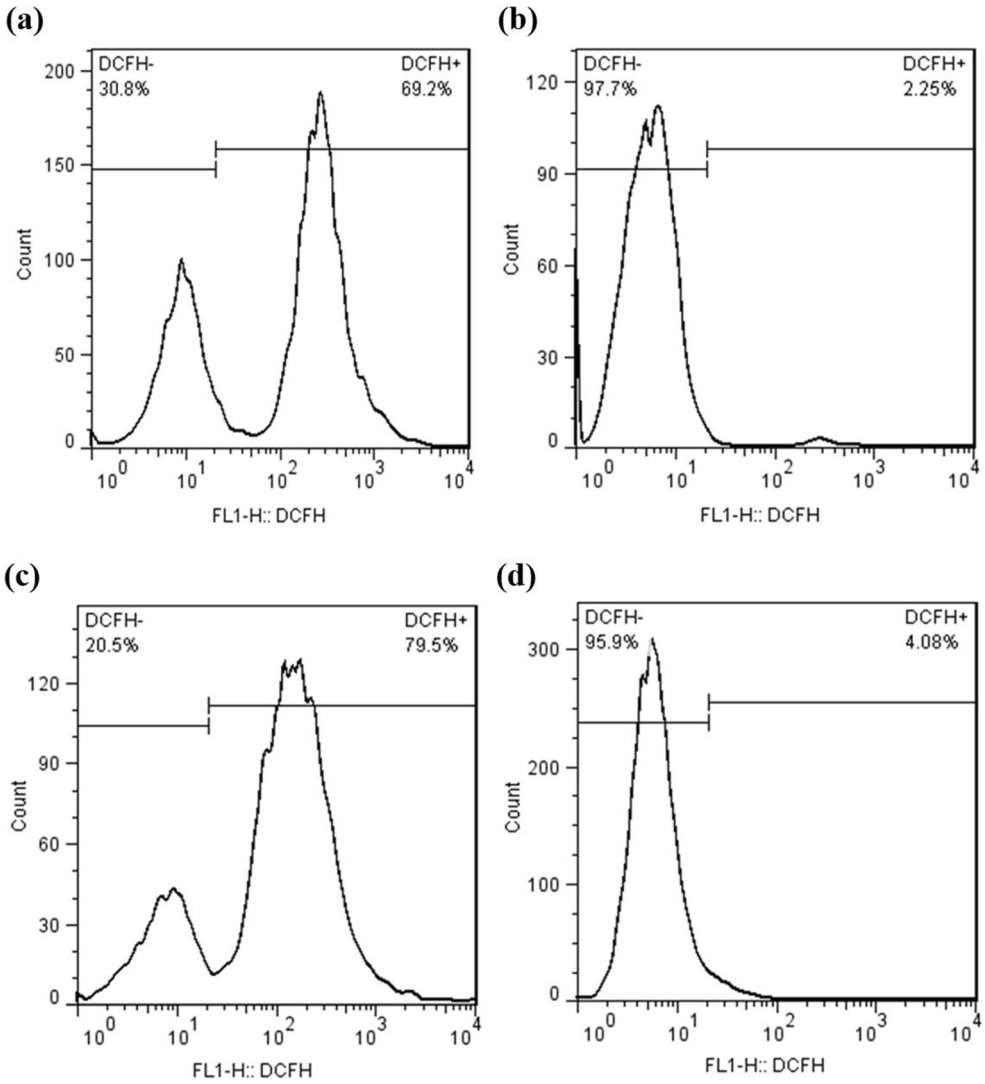

Fig. 6 Production of intracellular reactive oxygen species (ROS) in human colon cancer (SW480) after treatment with 1.5-fold of IC50 concentration of ZIF-8 NPs (54.34 μg mL^{-1}) for 24 h (a) relative to 0 mg L^{-1} of ZIF-8 NPs (control) (b) and in human embryonic kidney (HEK293) cell treated with 1.5-fold of IC50 concentration of ZIF-8 NPs (174.33 μg mL^{-1}) (c) compared with a control group (d)

A549 cells showed that this composite inhibited the growth of cancer cells via ROS-mediated cell cycle arrest and apoptosis (Jin et al. 2020).

The Annexin V-FITC/PI staining analysis and flow cytometry were used to evaluate ZIF-8 NP-induced necrosis/apoptosis in human colon cancer (SW480) and human embryonic kidney (HEK293) cells after 24-h treatment (Fig. 7). The results showed that 96.3% of the SW480 cells treated with ZIF-8 NPs (54.34 μg mL^{-1}) were in the early process of apoptosis and 2.13%, 0.73% and 0.8% of cells were in late of apoptosis, necrosis and viable stages, respectively. For HEK293 cells exposed to 174.33 μg mL^{-1} of ZIF-8 NPs, the percentages of cells in early apoptosis and late apoptosis were 45.9% and 35.2%, respectively, while the viable and necrotic cells percentages were observed to be 16.4% and 2.53%, respectively. The untreated SW480 and HEK293 cells as control groups exhibited the 98.6% and 95.9% of viable cells, respectively (Fig. 7). These results indicated that the experimental conditions were appropriate for exposure of cells to ZIF-8 NPs. Following exposure to ZIF-8 NPs for 24 h, the SW480 cells showed greater percentage of apoptotic cells compared with the HEK293 cells, indicating the higher toxicity of ZIF-8 NPs toward human colon cancer cells than the human normal cells. In contrast to our results, Jin et al. (2020) found that the apoptosis rate of human lung cancer A549 cells exposed to ZIF-8 (130 nm) for 24 h was 8.09%. The findings of current study reveal that ZIF-8 NPs can exert their cancer chemo-preventive effect through increasing apoptosis.

Conclusion

In this study, we synthetized nanoscale zinc imidazolate framework 8 particles and evaluated their cytotoxicity on two eukaryotic cell lines including human embryonic kidney (HEK293) and human colon cancer (SW480) cells. We determined that toxicity of ZIF-8 NPs on both cell lines increased significantly coincident with elevation of exposure

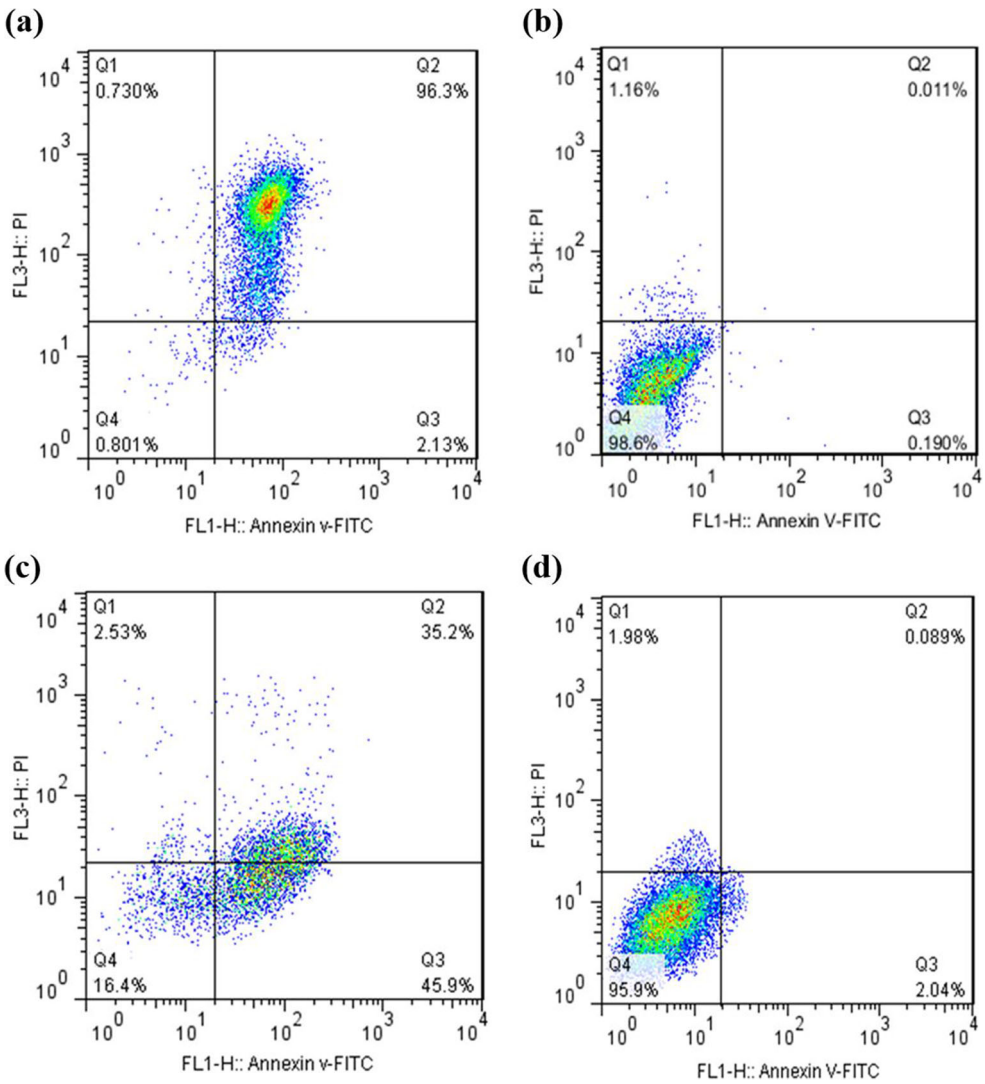

Fig. 7 Apoptosis/necrosis cells assay of human colon cancer (SW480) and human embryonic kidney (HEK293) cell lines using Annexin V-FITC/PI staining, and flow cytometry. SW480 cell exposed to 1.5-fold of IC50 concentration of ZIF-8 (54.34 μg mL^{-1}) for 24 h (a) compared with 0 mg L^{-1} of ZIF-8 NPs (control) (b). HEK293 cell exposed to 1.5-fold of IC50 concentration of ZIF-8 (174.33 μg mL^{-1}) (c) compared with a control group (d). Upper left quadrant represents the necrotic cells (Q1), upper right quadrant shows the late apoptosis cells (Q2), lower right quadrant indicates the early apoptosis cells (Q3) and lower left quadrant shows the viable cells (Q4)

concentration from 0 to 500 μg mL^{-1}. We also found that ZIF-8 NPs induced more reduction in viability of human colon cancer cells in comparison with human embryonic kidney cells. Our results indicated that an increase in the number of dead cells exposed to ZIF-8 NPs correlates with an increase in generation of ROS and activation of apoptosis pathway. Exposure of both cells to ZIF-8 NPs showed that the percentage of colon cancer SW480 cells in early apoptosis stages was clearly higher than that observed in the normal HEK293 cells. These results suggest that ZIF-8 NPs can be used as an antineoplastic agent, although they may show toxic effect on the normal cells at high concentrations.

Author contribution SAJ: investigation, supervision, conceptualization, methodology, funding acquisition, project administration, writing–review and editing; MS: conceptualization, data curation, writing–original draft preparation; SV: investigation.

Funding This work was supported by the University of Kurdistan (Grant number: GRC98-06503-1).

Data availability All data and materials are included in this published article.

Declarations

Ethics approval and consent to participate not applicable

Consent for publication Not applicable

Competing interests The authors declare no competing interests.

References

Bigdeli R, Shahnazari M, Panahnejad E, Cohan RA, Dashbolaghi A, Asgary V (2019) Cytotoxic and apoptotic properties of silver chloride nanoparticles synthesized using *Escherichia coli* cell-free supernatant on human breast cancer MCF 7 cell line. Artif Cells Nanomed Biotechnol 47(1):1603–1609

Cadet J, Wagner JR (2013) DNA base damage by reactive oxygen species, oxidizing agents, and UV radiation. Cold Spring Harb Perspect Biol 5(2):a012559. https://doi.org/10.1101/cshperspect.a012559

Chen X, Shi Z, Tong R, Ding S, Wang X, Wu J, Lei Q, Fang W (2018) A derivative of epigallocatechin-3-gallatea encapsulated in ZIF-8 with PEG-FA modification for target and pH responsive drug release in anticancer research. ACS Biomater Sci Eng 4(12):4183–4192

Chuah LH, Roberts CJ, Billa N (2014) Cellular uptake and anticancer effects of mucoadhesive curcumin-containing chitosan nanoparticles. Colloids Surf B: Biointerfaces 116:228–236

Clausen A, McClanahan T, Ji SG, Weiss JH (2013) Mechanisms of rapid reactive oxygen species generation in response to cytosolic Ca^{2+} or Zn^{2+} loads in cortical neurons. PLoS One 8(12):e83347. https://doi.org/10.1371/journal.pone.0083347

Costello LC, Franklin RB (2013) A review of the current status and concept of the emerging implications of zinc and zinc transporters in the development of pancreatic cancer. Pancreat Disord Ther 4:002. https://doi.org/10.4172/2165-7092.S4-002

De Jong WH, Borm PJ (2008) Drug delivery and nanoparticles: applications and hazards. Int J Nanomedicine 3:133

Dineley KE, Votyakova TV, Reynolds IJ (2003) Zinc inhibition of cellular energy production: implications for mitochondria and neurodegeneration. J Neurochem 85:563–570

Ding YS, Wang H, Niu JJ, Luo MY, Gou YM, Miao LN, Zou Z, Cheng Y (2016) Induction of ROS overload by alantolactone prompts oxidative DNA damage and apoptosis in colorectal cancer cells. Int J Mol Sci 17:558

Fang X, Zong B, Mao S (2018) Metal-organic framework-based sensors for environmental contaminant sensing. Nano Lett 10:64. https://doi.org/10.1007/s40820-018-0218-0

Grall R, Hidalgo T, Delic J, Garcia-Marquez A, Chevillard S, Horcajada P (2015) In vitro biocompatibility of mesoporous metal (III; Fe, Al, Cr) trimesate MOF nanocarriers. J Mater Chem B3:8279–8292

Heath JR, Davis ME (2008) Nanotechnology and cancer. Annu Rev Med 59:251–265. https://doi.org/10.1146/annurev.med.59.061506.185523

Hoang BX, Han B, Shaw DG, Nimni M (2016) Zinc as a possible preventive and therapeutic agent in pancreatic, prostate, and breast cancer. Eur J Cancer Prev 25:457–461

Hoop M, Walde CF, Riccò R, Mushtaq F, Terzopoulou A, Chen XZ, de Mello AJ, Doonan CJ, Falcaro P, Nelson BJ, Puigmartí-Luis J, Pané S (2018) Biocompatibility characteristics of the metal organic framework ZIF-8 for therapeutical applications. Appl Mater Today 11:13–21. https://doi.org/10.1016/j.apmt.2017.12.014

Huang L, Wu B, Wu Y, Yang Z, Yuan T, Alhassan SI, Yang W, Wang H, Zhang L (2020) Porous and flexible membrane derived from ZIF-8-decorated hyphae for outstanding adsorption of Pb^{2+} ion. J Colloid Interface Sci 565:465–473

Jampa SSK, Unnarkat AP, Vanshpati R, Pandian S, Sinha MK, Dharaskar S (2020) Adsorption and recyclability aspects of humic acid using nano-ZIF-8 adsorbent. Environ Technol Innov 19:100927

Jaracz S, Chen J, Kuznetsova LV, Olima I (2005) Recent advances in tumor targeting anticancer drug conjugates. Bioorg Med Chem 13:5043–5054 https://goo.gl/1grgtq

Jin S, Weng L, Li Z, Yang Z, Zhu L, Shi J, Tang W, Ma W, Zong H, Jiang W (2020) Nanoscale dual-enzyme cascade metal-organic frameworks through biomimetic mineralization as a ROS generator for synergistic cancer therapy. J Mater Chem B 8:4620–4626. https://doi.org/10.1039/D0TB00357C

Khan A, Jawaid M, Asiri AMA, Ni W, & Rahman MM (Eds.). (2020). Metal-organic framework nanocomposites: from design to application (1st ed.). 335 p. CRC Press. https://doi.org/10.1201/9780429346262

Kobayashi H, Watanabe R, Choyke PL (2014) Improving conventional enhanced permeability and retention (EPR) effects; what is the appropriate target? Theranostics 4(1):81–89

Kumar M, Sharma G, Kumar R, Singh B, Katare OP, Raza K (2018) Lysine-based C-60-fullerene nanoconjugates for monomethyl fumarate delivery: a novel nanomedicine for brain cancer cells. ACS Biomater Sci Eng 4(6):2134–2142. https://doi.org/10.1021/acsbiomaterials.7b01031

Li Q, Liu CG, Yu Y (2015) Separation of monodisperse alginate nanoparticles and effect of particle size on transport of vitamin E. Carbohydr Polym 124:274–279

Li L, Pang X, Liu G (2018) Near-infrared light-triggered polymeric nanomicelles for cancer therapy and imaging. ACS Biomater Sci Eng 4(6):1928–1941. https://doi.org/10.1021/acsbiomaterials.7b00648

Li N, Zhou L, Jin X, Owens G, Chen Z (2019) Simultaneous removal of tetracycline and oxytetracycline antibiotics from wastewater using a ZIF-8 metal organic-framework. J Hazard Mater 366:563–572

Link TA, von Jagow G (1995) Zinc ions inhibit the QP center of bovine heart mitochondrial bc1 complex by blocking a protonatable group. J Biol Chem 270:25001–25006

Liu X, Gao C, Gu J, Jiang Y, Yang X, Li S, Gao W, An T, Duan H, Fu J, Wang Y, Yang X (2016) Hyaluronic acid stabilized iodine-containing nanoparticles with Au nanoshell coating for X-ray CT imaging and photothermal therapy of tumors. ACS Appl Mater Interfaces 8(41):27622–27631. https://doi.org/10.1021/acsami.6b11918

Liu M, Qian Y, Deng Z, Zhao P, Shen J (2018) Multifunctional core/shell hybrid Fe3O4@TiO2@ZIF-8 nanoparticles as a pH-responsive vehicle advances in targeted cancer therapeutics. Am J Nanotechnol Nanomed 1(1):016–027

Liu F, Xiong W, Feng X, Shi L, Chen D, Zhang Y (2019) A novel monolith ZnS-ZIF-8 adsorption material for ultra-effective Hg (II) capture from wastewater. J Hazard Mater 367:381–389

Maeda H (2001) The enhanced permeability and retention (EPR) effect in tumor vasculature: the key role of tumor-selective macromolecular drug targeting. Adv Enzym Regul 41:189–207

Nabipour H, Hossaini S, Rezanejade Bardajee G (2017) Synthesis and characterization of nanoscale zeolitic imidazolate frameworks with ciprofloxacin and their applications as antimicrobial agents. New J Chem 41:7364–7370. https://doi.org/10.1039/C7NJ00606C

Nel A, Mädler L, Velegol D, Xia T, Hoek EMV, Somasundaran P, Klaessig F, Castranova V, Thompson M (2009) Understanding biophysicochemical interactions at the nano–bio interface. Nat Mater 8:543–557. https://doi.org/10.1038/nmat2442

Pavithra V, Sathisha TG, Kasturi K, Mallika DS, Amos SJ, Ragunatha S (2015) Serum levels of metal ions in female patients with breast cancer. J Clin Diagn Res 9:BC25–BC27

Peng S, Bie B, Sun Y, Liu M, Cong H, Zhou W, Xia Y, Tang H, Deng H, Zhou X (2018) Metal organic frameworks for precise inclusion of single-stranded DNA and transfection in immune cells. Nat Commun 9:9. https://doi.org/10.1038/s41467-018-03650-w

Ran J, Wang C, Zhang J, Wang W, Xiao L, Jia S, Wang S, Wu W, Xiao J, Wu X (2018) New insight into polydopamine@ZIF-8 nanohybrids: a zinc-releasing container for potential anticancer activity. Polymers 10:476. https://doi.org/10.3390/polym10050476

Sajid M (2016) Toxicity of nanoscale metal organic frameworks: a perspective. Environ Sci Pollut Res 23:14805–14807

Salatin S, Yari Khosroushahi A (2017) Overviews on the cellular uptake mechanism of polysaccharide. J Cell Mol Med 21(9):1668–1686

Shu F, Lv D, Song XL, Huang B, Wang C, Yua Y, Zhao SC (2018) Fabrication of a hyaluronic acid conjugated metal organic framework for targeted drug delivery and magnetic resonance imaging. RSC Adv 8:6581–6589

Shyamsivappan S, Vivek R, Saravanan A, Arasakumar T, Suresh T, Athimoolam S, Mohan PS (2020) A novel 8-nitro quinoline-thiosemicarbazone analogues induces G1/S & G2/M phase cell cycle arrest and apoptosis through ROS mediated mitochondrial pathway. Bioorg Chem 97:103709. https://doi.org/10.1016/j.bioorg.2020.103709

Song Y, Ho E (2009) Zinc and prostatic cancer. Curr Opin Clin Nutr Metab Care 12:640–645

Sun CY, Qin C, Wang XL, Guang SY, Kui ZS, Ya QL (2012) Zeolitic imidazolate framework-8 as efficient pH-sensitive drug delivery vehicle. Dalton Trans 41:6906–6909

Taheria M, Ashoka D, Sen T, Gabriel Enge T, K.Verma N, Tricoli A, Lowe A, Nisbet DR, Tsuzuki T (2021) Stability of ZIF-8 nanopowders in bacterial culture media and its implication for antibacterial properties. Chem Eng J 413;127511. https://doi.org/10.1016/j.cej.2020.127511

Tamames-Tabar C, Cunha D, Imbuluzqueta E, Ragon F, Serre C, Blanco-Prieto MJ, Horcajada P (2014) Cytotoxicity of nanoscaled metal–organic frameworks. J Mater Chem B 2:262–271

Tiwari A, Singh A, Garg N, Randhawa J (2017) Curcumin encapsulated zeolitic imidazolate frameworks as stimuli responsive drug delivery system and their interaction with biomimetic environment. Sci Rep 7:12598. https://doi.org/10.1038/s41598-017-12786-6

Vasconcelos IB, da Silva TG, Militao GCG, Soares TA, Rodrigues NM, Rodrigues MO, da Costa NB, Freire RO, Junior SA (2012) Cytotoxicity and slow release of the anti-cancer drug doxorubicin from ZIF-8. RSC Adv 2:9437–9442

Wang T, Bai J, Jiang X (2012) Cellular uptake of nanoparticles by membrane penetration: a study combining confocal microscopy with FTIR spectroelectrochemistry. ACS Nano 6:1251–1259

Wang D, Zhou J, Shi R, Wu H, Chen R, Duan B, Xia G, Xu P, Wang H, Zhou S, Wang C, Wang H, Guo Z, Chen Q (2017) Biodegradable core-shell dual-metal-organic-frameworks nanotheranostic agent for multiple imaging guided combination cancer therapy. Theranostics 7(18):4605–4617. https://doi.org/10.7150/thno.20363

Wasim L, Chopra M (2018) Synergistic anticancer effect of panobinostat and topoisomerase inhibitors through ROS generation and intrinsic apoptotic pathway induction in cervical cancer cells. Cell Oncol 41:201–212. https://doi.org/10.1007/s13402-017-0366-0

Wicki A, Witzigmann D, Balasubramanian V, Huwyler J (2015) Nanomedicine in cancer therapy: challenges, opportunities, and clinical applications. J Control Release 200:138–157

Zarogoulidis P, Chatzaki E, Porpodis K, Domvri K, Hohenforst SW, Goldberg EP (2012) Inhaled chemotherapy in lung cancer: future concept of nanomedicine. Int J Nanomedicine 7:1551–1572

Zheng M, Liu S, Guan X, Xie Z (2015) One-step synthesis of nanoscale zeolitic imidazolate frameworks with high curcumin loading for treatment of cervical cancer. ACS Appl Mater Interfaces 7(40):22181–22187. https://doi.org/10.1021/acsami.5b04315

Zheng H, Zhang Y, Liu L, Wan W, Guo P, Nyström AM, Zou X (2016) One-pot synthesis of metal-organic frameworks with encapsulated target molecules and their applications for controlled drug delivery. J Am Chem Soc 138(3):962–968. https://doi.org/10.1021/jacs.5b11720

Zhou L, Li N, Owens G, Chena Z (2019) Simultaneous removal of mixed contaminants, copper and norfloxacin, from aqueous solution by ZIF-8. Chem Eng J 362;628–637. https://doi.org/10.1016/j.cej.2019.01.068

Zhuang J, Kuo CH, Chou LY, Liu DY, Weerapana E, Tsung CK (2014) Optimized metal-organic-framework nanospheres for drug delivery: evaluation of small-molecule encapsulation. ACS Nano 8:2812–2819